PHYSICAL REVIEW B **106**, 125122 (2022)

Tuning the magnetic anisotropy and topological phase with electronic correlation in single-layer H-FeBr$_2$

Weiyi Pan[*]
State Key Laboratory of Low Dimensional Quantum Physics and Department of Physics, Tsinghua University, Beijing 100084, China

(Received 7 May 2022; revised 22 July 2022; accepted 7 September 2022; published 14 September 2022)

Electronic correlation can strongly influence the electronic properties of two-dimensional (2D) materials with open d or f orbitals. Herein, by taking single-layer (SL) H-FeBr$_2$ as a representative of the SL H-FeX$_2$ (X = Cl, Br, I) family, we investigated the electronic correlation effects in the magnetic anisotropy and electronic topology of such a system based on first-principles calculations with the density functional theory $+U$ approach. Our result is that the magnetic anisotropy energy (MAE) of SL H-FeBr$_2$ shows a nonmonotonic evolution behavior with increasing electronic correlation strength, which is mainly due to the competition between different element-resolved MAEs of Fe and Br. Further investigations show that the evolution of element-resolved MAE arises from the variation of the spin-orbital coupling interaction between different orbitals in each atom. Moreover, tuning the strength of the electronic correlation can drive the occurrence of band inversions, causing the system to undergo multiple topological phase transitions and resulting in a quantum anomalous valley Hall effect. These exotic properties are universal for the SL H-FeX$_2$ (X = Cl, Br, I) family. Our work sheds light on the role of electronic correlation effects in tuning magnetic and electronic structures in the SL H-FeX$_2$ (X = Cl, Br, I) family, which could guide advances in the development of new spintronics and valleytronics devices based on these materials.

DOI: 10.1103/PhysRevB.106.125122

I. INTRODUCTION

Electrons in materials with open d or f shells possess an electronic correlation that would significantly affect the electronic structure in materials and give rise to a variety of exotic properties such as electronic topology [1–5], magnetism [6–8], and metal-insulator transitions [9–11]. Generally, electron correlation effects are more pronounced in two-dimensional (2D) systems than in 3D systems with the same chemical composition. This is because Coulomb screening, which suppresses the long-range Coulomb interaction between electrons, is inhibited by dimensionality reduction in 2D systems. Therefore, it is easier to tune the electronic correlation strength of 2D systems experimentally, e.g., through the use of a structured substrate [12–14] or the growth of multilayer films with different thicknesses [15]. However, the properties developed by Coulomb engineering have been theoretically revelled in 2D materials [10,11,16,17]. For example, a coexisting quantum anomalous Hall insulating state in a VSi$_2$P$_4$ monolayer can be induced by tuning the Hubbard U constant in first-principles calculations [17]. By varying the Coulomb repulsion U, the location of the metal-insulator transition and the magnetism as well as the superconductivity of some 2D systems were revealed [10]. Thus, 2D materials provide a good playground to investigate numerous electronic correlation effects.

Recently, a new class of 2D van der Waals systems, single-layer (SL) H-FeX$_2$ (X = Cl, Br, I) [18–20], has attracted much attention. It has been reported that SL H-FeCl$_2$ is a ferrovalley (FV) material [21] with spontaneous valley polarization coupled with ferromagnetism (FM). Theoretical calculations have shown that the easy magnetization axis of SL H-FeClF would rotate from out-of-plane to in-plane [22] by increasing the strength of the electronic correlation (U_{eff}). In addition, the electronic energy bands of SL H-FeClF exhibit a noticeable evolution with U_{eff}, giving rise to topological phase transitions [22]. Intuitively, varying the strength of electronic correlations alters the local distribution of electronic valence charges on the open d shell of Fe ions and changes the local magnetism as well as the strength of spin-orbital coupling (SOC). This, of course, drives the evolution of the atomic-scale magnetic anisotropy (MA) of the system. As we know, the atomic-scale MA is not only tightly related to the performance of the upper limit of the system's magnetic memory but also in connection with the polarization of valleys in FV materials due to magneto-valley coupling [17,23]. Therefore, it is necessary to study the MA of SL H-FeX$_2$ (X = Cl, Br, I). Unfortunately, the evolutionary behavior of MA with U_{eff} of SL H-FeX$_2$ (X = Cl, Br, I) members is unknown. In addition, since the modulation of both the electronic structure and the magnetic properties in each member of the SL H-FeX$_2$ (X = Cl, Br, I) family is driven by the Coulomb correlation on Fe, the performance of MA in each member of the family would likely share a common trait. On the other hand, different members of SL H-FeX$_2$ (X = Cl, Br, I) have different halogen elements, and these different halogen elements would, to some extent, alter

---

[*] pwy20@mails.tsinghua.edu.cn

the modulation of the electronic and magnetic properties of the system in different manners. The study of these concerns is clearly of great importance in both the scientific interest and the technological importance of spintronics.

In this work, we investigated the effect of electronic correlation on electronic structures as well as the magnetic anisotropy energy (MAE), represented by SL H-FeBr$_2$. Based on the first-principles calculations with the density-functional theory (DFT)+U approach, we found that the trend of MAE with increasing value of U_{eff} imposed on Fe shows a nonmonotonic evolution behavior corresponding to a flip between in-plane and out-of-plane magnetization. We suggested that this nonmonotonic evolutionary behavior of MAE is attributed to the competition between the element-resolved MAE contributed by Fe and Br atoms. The above-mentioned MAE behavior with U_{eff} and its underlying mechanism is universal for the SL H-FeX$_2$ (X = Cl, Br, I) family. In addition, band inversion occurs in SL H-FeBr$_2$ during the rise of U_{eff}, leading to occurrence of topological phase transitions and quantum anomalous valley Hall (QAVH) states. Our work highlights the correlation effects on the MAE and the topological phase transition in H-FeX$_2$ (X = Cl, Br, I) family.

II. METHODS

We performed first-principles DFT calculations implemented in the Vienna *ab initio* Simulations Package [24] to study all our concerns in the present work. In our theoretical treatment, the plane-wave cutoff energy was set to be 600 eV and the Brillouin zone was sampled with a 12 × 12 × 1 Γ-centered k-point mesh. The generalized gradient approximation with the Perdew-Burke-Ernzerhof realization was used for the exchange correlation functional [25]. To treat the effect of the correlation between electrons in the 3d orbitals of Fe atoms, the Dudarev's approach of Coulomb correction implemented in the DFT + U scheme was applied to Fe ions in the system, where only $U_{\text{eff}} = U - J$ is meaningful (Dudarev's approach) [26]. In addition, the vdW correction included in the DFT-D3 method was considered [27]. During structural optimization, both the atomic positions and the lattice constants of each system were fully relaxed until the Hellmann-Feynman forces acting on each atom were less than 10^{-3} eV/Å; The electronic convergence criteria was set to be 10^{-6} eV. Since our concerned system is a two-dimensional nanosheet, a vacuum region of 20 Å along the direction perpendicular to the surface of the nanosheet was added to avoid the interaction between the periodic images. To calculate the Berry curvature, the maximally localized Wannier functions were constructed using the WANNIER90 package [28]. The edge states were calculated using the iterative Green function method, which is implemented in the WANNIERTOOLS package [29].

The MAE is defined as the total energy difference between the in-plane FM configuration (E_x) and the out-of-plane FM configuration (E_z), namely

$$\text{MAE} = E_x - E_z. \tag{1}$$

Here the positive or negative value of MAE indicates that the magnetization direction is along the out-of-plane or in-plane direction. Moreover, the element- and orbital-resolved MAEs were calculated from the difference in SOC energies between in-plane and out-of-plane ferromagnetic configurations [30], i.e.,

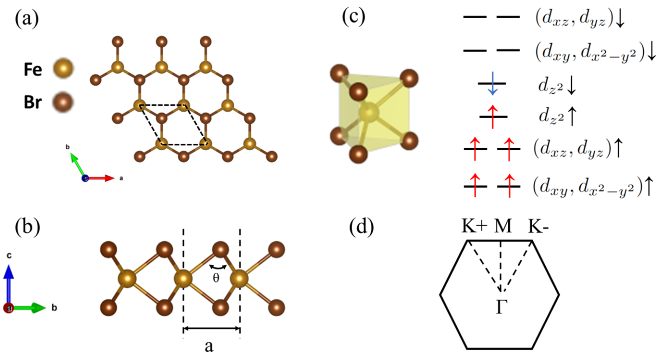

FIG. 1. (a) Top and (b) side view of the atomic structure of SL H-FeBr$_2$. (c) Splitting of the 3d orbitals of Fe atom under the trigonal prismatic crystal field. The trigonal prismatic crystal structure is also shown. (d) The Brillouin zone with high-symmetry points labeled.

$$\Delta E_{\text{SOC}} = E^x_{\text{SOC}} - E^z_{\text{SOC}}, \tag{2}$$

with

$$E_{\text{SOC}} = \left\langle \frac{h^2}{2m^2c^2}\frac{1}{r}\frac{dV}{dr}\hat{L}\cdot\hat{S} \right\rangle, \tag{3}$$

where $V(r)$ is the spherical part of the effective potential inside the PAW sphere, while $\hat{L}$ and $\hat{S}$ are the orbital and spin angular momentum, respectively. According to second-order perturbation theory, only approximately 50% of the SOC energy difference contributes to the MAE, i.e., MAE $\approx \frac{1}{2}\Delta E_{\text{SOC}}$ [31,32], and the remaining SOC energies might translate into both crystal-field energy and unquenched orbital moments [33].

III. RESULTS AND DISCUSSION

A. Basic structural and magnetic properties

The SL H-FeBr$_2$ has a hexagonal structure with the space group $P\bar{6}m2$ (No. 187). A Fe monolayer is sandwiched by two adjacent Br monolayers and each Fe atom is surrounded by six Br atoms, forming a local FeBr$_6$ trigonal prism, as shown in Figs. 1(a) and 1(b). Our calculations showed that the lattice constant of this system is $a = 3.57$ Å and that the bond angle of Fe-Br-Fe is $\theta = 85.3^\circ$, which are in excellent agreement with the literature [18]. In particular, the six Br ions in each FeBr$_6$ trigonal prism provide a local crystal field on each Fe atom [seen in Fig. 1(c)]. This causes the 3d orbitals of the Fe atom to split into three groups in the energy landscape: the d_{z^2} orbital (denoted as A_1), the degenerate ($d_{xy}, d_{x^2-y^2}$) orbitals (denoted as E_1), and the (d_{xz}, d_{yz}) orbitals (denoted as E_2), which are schematically displayed in Fig. 1(c). Since the electronic configuration of the Fe^{2+} ion is 3d^6, the spin-up channel of the 3d orbitals is fully occupied. For the spin-down channel, only the d_{z^2} orbital is occupied by an electron, and the other 3d orbitals are empty. This gives rise to a spin magnetic moment of 4μ_B on each Fe^{2+} ion.

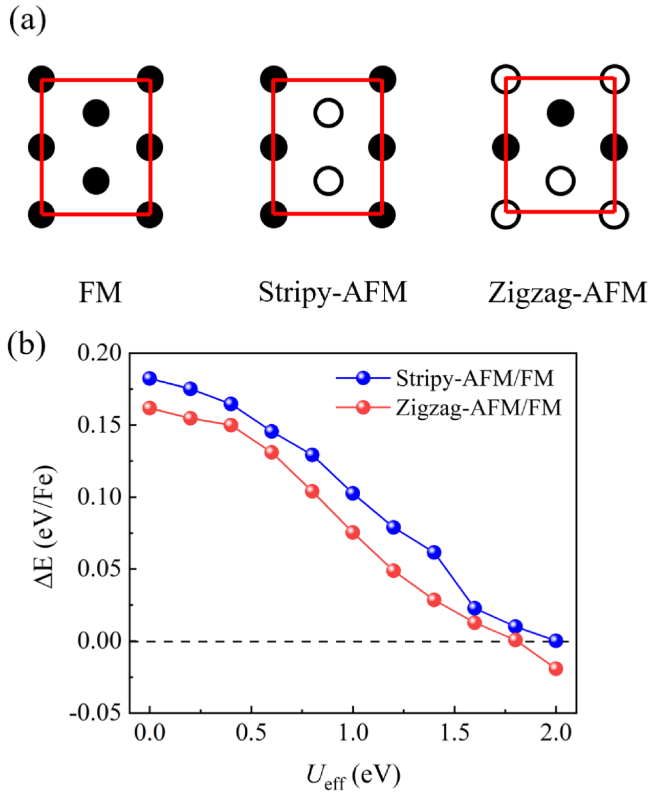

FIG. 2. (a) The schematic top views of the FM, stripy AFM, and zigzag AFM magnetic configurations. The solid and open circles represent spin-up and spin-down states, respectively. (b) The evolution of the energy difference between FM and stripy AFM (zigzag AFM) states with U_{eff}. The energy difference is defined as $\Delta E = E_{\text{Stripy/Zigzag}} - E_{\text{FM}}$, which is labeled as blue (red) dots.

To investigate the magnetic ground state of SL H-FeBr$_2$, three types of magnetic configurations, i.e., a FM configuration, a stripy antiferromagnetic (AFM) configuration and a zigzag AFM configuration [seen in Fig. 2(a)], were considered. By performing calculations of the nanosheet with each concerned magnetic configuration when U_{eff} is imposed on Fe and varied from 0.0 to 1.8 eV, we found that the energy of the system with either the stripy AFM or the zigzag AFM configuration is significantly higher than that with the FM configuration [Fig. 2(b)], which agrees well with the previous study [18].

The origin of the above FM state can be understood in terms of the superexchange interaction. Note that the bond angle (85.3°) of Fe-Br-Fe in SL H-FeBr$_2$ is close to 90°. Combining this structural feature with the Goodenough-Kanamori-Anderson rules [34,35], we know that the superexchange interaction between the two nearest-neighboring Fe atoms predominantly characterizes the feature of FM interaction. In addition to this FM superexchange interaction, there is also a direct AFM exchange between the two nearest-neighboring Fe ions. However, due to the localization of d orbitals on each magnetic atom, its strength is usually weaker than that of the FM superexchange interaction. Hence, the FM superexchange interaction dominates the interaction between the two nearest-neighboring Fe ions in SL H-FeBr$_2$ when U_{eff} is small.

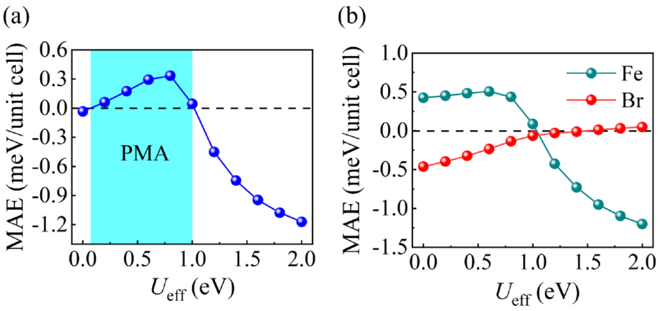

FIG. 3. The evolution of (a) total MAE and (b) element-resolved MAE in a unit cell with U_{eff}.

Another aspect shown in Fig. 2(b) is that the energy difference between the stripy AFM and FM configurations or between the zigzag AFM and FM configurations (defined as $\Delta E = E_{\text{Stripy/Zigzag}} - E_{\text{FM}}$) decreases with increasing value of U_{eff}, showing a weakening of FM coupling. When U_{eff} reaches 2.0 eV, the zigzag AFM configuration has a lower energy than that of the FM configuration, leading to an AFM ground state.

In fact, this FM-AFM transition behavior can be understood as a consequence of the competition between the indirect FM superexchange and the direct AFM exchange. As we know, the indirect FM superexchange strength is proportional to $-\frac{t_{pd}^4 J_H^p}{(\Delta_{pd}+U_d)^4}$, with t_{pd}, J_H^p, Δ_{pd}, and U_d representing the hybridization strength between Fe-d orbitals and Br $-$ p orbitals, the Hund's coupling strength of Br $-$ p orbitals, the energy interval between Fe-d orbitals and Br $-$ p orbitals, and the spin-splitting energy of Fe-d orbitals, respectively [36]. Meanwhile, the strength of direct AFM exchange is proportional to $\frac{t_{dd}^2}{U_d}$, with t_{dd} being the strength of direct hybridization between the d orbitals of the nearest-neighboring Fe ions.

With increasing U_{eff}, the spin splitting U_d increases significantly. The above formulas show that the indirect FM superexchange strength is inversely proportional to the fourth power of the U_d value, while the direct AFM exchange strength is only inversely proportional to the first power of the U_d value. Obviously, increasing the U_d value leads to a more pronounced decrease in the strength of the indirect FM superexchange than that of the direct AFM exchange. As a result, the energy difference between AFM and FM decreases with U_{eff}, giving rise to a transition between AFM and FM magnetic configurations.

We emphasize that although the energy of the zigzag AFM state is slightly lower than that of the FM state (approximately 0.007 eV/Fe) when $U_{\text{eff}} = 2.0$ eV, FM is the most energetically favorable state in most of the considered range (from 0.0 to 2.0 eV) of U_{eff}. Thus, in our following calculations, only the FM state of the system will be investigated.

B. Electronic correlation effects on MAE

Now we turn to investigate the evolution of MAE with different correlation strengths represented by U_{eff} in Fe. Figure 3 displays our calculated MAE as a function of U_{eff}. As shown in Fig. 3(a), the MAE value increases with increasing U_{eff} until the U_{eff} value reaches 0.8 eV, followed by a rapid decrease in MAE. Therefore, by increasing the value of U_{eff},

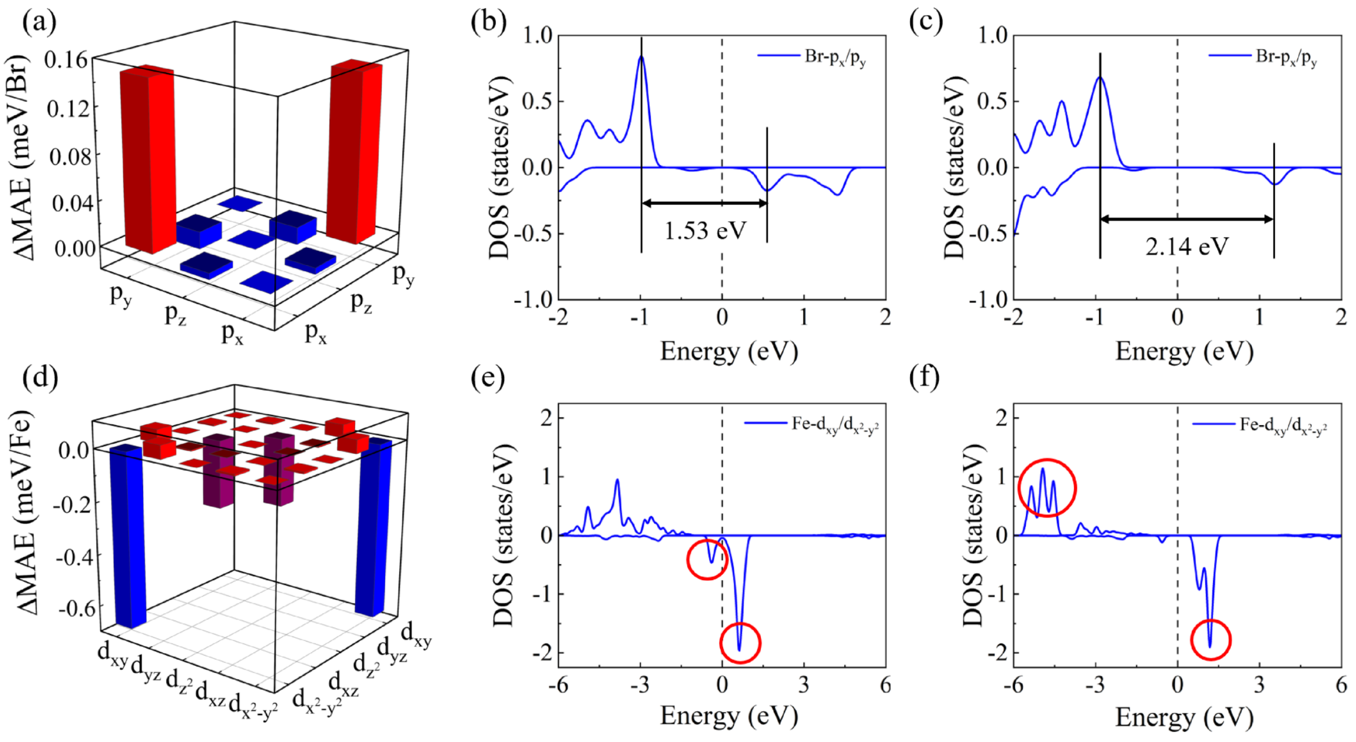

FIG. 4. (a) The difference in the orbital-resolved MAE of each Br atom between $U_{\mathrm{eff}} = 0.0\,\mathrm{eV}$ and $U_{\mathrm{eff}} = 2.0\,\mathrm{eV}$, which is defined as $\Delta\mathrm{MAE} = \mathrm{MAE}_{U_{\mathrm{eff}}=2.0\,\mathrm{eV}} - \mathrm{MAE}_{U_{\mathrm{eff}}=0.0\,\mathrm{eV}}$. The spin-polarized DOS of Br-p_x and Br-p_y orbitals at (b) $U_{\mathrm{eff}} = 0.0\,\mathrm{eV}$ and (c) $U_{\mathrm{eff}} = 2.0\,\mathrm{eV}$ is given. (d) The difference in the orbital-resolved MAE of each Fe atom between $U_{\mathrm{eff}} = 0.8\,\mathrm{eV}$ and $U_{\mathrm{eff}} = 2.0\,\mathrm{eV}$, which is defined as $\Delta\mathrm{MAE} = \mathrm{MAE}_{U_{\mathrm{eff}}=2.0\,\mathrm{eV}} - \mathrm{MAE}_{U_{\mathrm{eff}}=0.8\,\mathrm{eV}}$. The spin-polarized DOSs of the Fe $- d_{xy}$ and Fe -$d_{x^2-y^2}$ orbitals at (e) $U_{\mathrm{eff}} = 0.8\,\mathrm{eV}$ and (f) $U_{\mathrm{eff}} = 2.0\,\mathrm{eV}$ are given.

the MAE varies from negative values to positive values and then to negative values again. This corresponds to the change of the magnetic state from the out-of-plane FM state to the in-plane FM state before returning to the out-of-plane FM state. The system prefers an in-plane FM state if U_{eff} <0.1 eV or U_{eff} >1.0 eV. Otherwise, the system shows an out-of-plane FM state. Therefore, there exists a perpendicular magnetic anisotropy (PMA) in the range of 0.1 eV <U_{eff}<1.0 eV.

Basically, the entire MAE of the system is contributed from each atom. Thus, the element-resolved MAE as a function of U_{eff} was calculated, which is shown in Fig. 3(b). Remarkably, the MAE from Fe and Br elements show a completely different behavior with increasing U_{eff}: The MAE of Br (denoted as Br-MAE) increases monotonically with increasing U_{eff}; however, the MAE of Fe (denoted as Fe-MAE) remains almost constant before U_{eff} reaches 0.8 eV, and when $U_{\mathrm{eff}} > 0.8\,\mathrm{eV}$, Fe-MAE decreases sharply and varies from positive values to negative values. Apparently, the nonmonotonic behavior of the whole MAE in a unit cell could be the result of the competition of the element-resolved MAE between Fe and Br. For U_{eff}<0.8 eV, the enhancement of Br-MAE dominates, which is responsible for the increase in the total MAE. For U_{eff} >0.8 eV, the faster change in the Fe-MAE dominates and gives rise to a decrease in the total MAE.

Why does the evolution of Br-MAE behave differently than that of Fe-MAE with changing U_{eff}? To uncover the nature underlying this concern, we recall that based on the second-order perturbation theory, the MAE essentially correlates with the SOC interaction between the occupied and unoccupied states around the Fermi level, which is expressed as [37,38]

$$\mathrm{MAE} = \sum_{\sigma,\sigma'}(2\delta_{\sigma,\sigma'} - 1)\xi^2 \times \sum_{o^\sigma,u^{\sigma'}} \frac{|\langle o^\sigma|\hat{L}_z|u^{\sigma'}\rangle|^2 - |\langle o^\sigma|\hat{L}_x|u^{\sigma'}\rangle|^2}{E_u^{\sigma'} - E_o^\sigma}. \quad (4)$$

Here ξ is the strength of SOC, and σ and σ' are spin indexes. $\hat{L}_z$ and $\hat{L}_x$ are angular momentum operators. $|o^\sigma\rangle$ ($|u^{\sigma'}\rangle$) is the occupied (unoccupied) state with spin σ (σ'), whose energy is E_o^σ ($E_u^{\sigma'}$). According to the expression above, the MAE is sensitive to the energy interval between occupied and unoccupied states, $E_u^{\sigma'} - E_o^\sigma$. Thus, by tuning the value of U_{eff}, the value of $E_u^{\sigma'} - E_o^\sigma$ could change, giving rise to the variation in MAE.

Furthermore, we computed the orbital-resolved MAE for each Br atom with U_{eff}= 0.0 eV and 2.0 eV and for each Fe atom with $U_{\mathrm{eff}} = 0.8\,\mathrm{eV}$ and 2.0 eV (as shown in Fig. S1 in the Supplemental Material [39]), followed by making difference $\Delta\mathrm{MAE} = \mathrm{MAE}_{U_{\mathrm{eff}}=2.0\,\mathrm{eV}} - \mathrm{MAE}_{U_{\mathrm{eff}}=0.0\,\mathrm{eV}}$ for Br and $\Delta\mathrm{MAE} = \mathrm{MAE}_{U_{\mathrm{eff}}=2.0\,\mathrm{eV}} - \mathrm{MAE}_{U_{\mathrm{eff}}=0.8\,\mathrm{eV}}$ for Fe, as displayed in Figs. 4(a) and 4(d).

In the case of Br, it is observed in Fig. 4(a) that as the value of U_{eff} increases from 0.0 eV to 2.0 eV, the $p_x - p_y$ orbital pairs make more positive contributions to the Br-MAE, while those from other orbital pairs have only minor contributions, thus only the Br-p_x and Br-p_y orbitals are considered. To understand the phenomenon observed above, we calculated the density of states (DOS) of spin-polarized Br-p_x and Br-p_y orbitals in SL H-FeBr$_2$ when $U_{\mathrm{eff}} = 0.0$ eV and $U_{\mathrm{eff}} = 2.0$ eV, which are shown in Fig. 4(b) and 4(c). It can be observed that the p_x and p_y orbitals of Br are all degenerate. Furthermore, the unoccupied states of Br near the Fermi level are dominated by the spin-down $p_{x/y}$ states and the occupied states of Br near the Fermi level are dominated by the spin-up $p_{x/y}$ states.

We first investigate the MAE contributed by the SOC interaction between the unoccupied spin-down Br-p_y states (denoted as $|p^{\downarrow}_{y,u}\rangle$) and the occupied spin-up Br-p_x states (denoted as $|p^{\uparrow}_{x,o}\rangle$), which can be expressed as:

$$\mathrm{MAE}_{\mathrm{Br}-p_{x/y}} = -\xi^2 \sum_{o,u} \frac{|\langle p^{\uparrow}_{x,o}|\hat{L}_z|p^{\downarrow}_{y,u}\rangle|^2 - |\langle p^{\uparrow}_{x,o}|\hat{L}_x|p^{\downarrow}_{y,u}\rangle|^2}{E^{\downarrow}_{p_{y,u}} - E^{\uparrow}_{p_{x,o}}}. \tag{5}$$

Note that the matrix elements are [40]

$$\langle p_x|\hat{L}_z|p_y\rangle = i \tag{6}$$

and

$$\langle p_x|\hat{L}_x|p_y\rangle = 0. \tag{7}$$

Thus, the $\mathrm{MAE}_{\mathrm{Br}-p_{x/y}}$ can be simplified as:

$$\mathrm{MAE}_{\mathrm{Br}-p_{x/y}} = -\xi^2 \sum_{o,u} \frac{1}{E^{\downarrow}_{p_{y,u}} - E^{\uparrow}_{p_{x,o}}}. \tag{8}$$

Apparently, the $\mathrm{MAE}_{\mathrm{Br}-p_{x/y}}$ contributes to the negative value of Br-MAE. We can further divide the $\mathrm{MAE}_{\mathrm{Br}-p_{x/y}}$ into two parts, namely the contributions from the SOC interaction between the highest occupied (HO) spin-up Br-p_x states and the the lowest unoccupied (LU) spin-down Br-p_y states, as well as the contributions from the SOC interaction between other unoccupied spin-down Br-p_y states and occupied spin-up Br-p_x states:

$$\begin{aligned}\mathrm{MAE}_{\mathrm{Br}-p_{x/y}} = &-\xi^2 \frac{1}{E^{\downarrow}_{p_{y,\mathrm{LU}}} - E^{\uparrow}_{p_{x,\mathrm{HO}}}}\\ &-\xi^2 \sum_{o,u,\mathrm{other}} \frac{1}{E^{\downarrow}_{p_{y,u}} - E^{\uparrow}_{p_{x,o}}}.\end{aligned} \tag{9}$$

Since the energy difference between the HO spin-up Br-p_x state and the LU spin-down Br-p_y state is the smallest among all the unoccupied spin-down Br-p_y states and occupied spin-up Br-p_x states, the $\mathrm{MAE}_{\mathrm{Br-p_{x/y}}}$ is dominated by the first term, i.e., $-\xi^2\frac{1}{E^{\downarrow}_{p_{y,\mathrm{LU}}}-E^{\uparrow}_{p_{x,\mathrm{HO}}}}$, which is tightly correlated to the energy difference, $E^{\downarrow}_{p_{y,\mathrm{LU}}} - E^{\uparrow}_{p_{x,\mathrm{HO}}}$. Here the value of $E^{\downarrow}_{p_{y,\mathrm{LU}}} - E^{\uparrow}_{p_{x,\mathrm{HO}}}$ can be approximately reflected in the energy difference between the two major peaks in the DOS of occupied spin-up Br-p_x states and unoccupied spin-down Br-p_y states near the Fermi level, as shown in Figs. 4(b) and 4(c).

After adjusting the value of U_{eff} from 0.0 to 2.0 eV, the aforementioned energy difference was changed from 1.53 to 2.14 eV. This increase in the energy difference gives rise to a smaller magnitude of negative $\mathrm{MAE}_{\mathrm{Br-p_{x/y}}}$, which is responsible for the increase in Br-MAE.

We recall that the p_x and p_y orbitals of Br are degenerate, and thus it is reasonable to perform the same analysis on the unoccupied spin-down p_x states and the occupied spin-up p_y states of Br near the Fermi level. By investigating the features of DOS corresponding to these two states, we found that the gap width between the main peaks in the DOS corresponding to these two orbitals increase as well, resulting in a decreasing magnitude in the negative Br-MAE. Therefore, the Br-MAE increases with U_{eff}.

For Fe, Fig. 4(d) shows that as the value of U_{eff} increases from 0.8 to 2.0 eV, the $d_{xy} - d_{x^2-y^2}$ orbital pairs make more negative contributions to the Fe-MAE, and those from other orbital pairs have minor contributions, and thus only the $d_{x^2-y^2}$ and d_{xy} orbitals of Fe are considered. To explain this phenomenon, the spin-polarized DOSs of the Fe-$d_{x^2-y^2}$ orbital and Fe-d_{xy} orbital in SL H-FeBr$_2$ are calculated when $U_{\mathrm{eff}} =$ 0.8 eV and 2.0 eV, respectively, which are shown in Figs. 4(e) and 4(f). It is easy to find that the d_{xy} and $d_{x^2-y^2}$ orbitals of Fe are degenerate.

In the case of $U_{\mathrm{eff}} = 0.8$ eV, the major Fe-$d_{xy}/d_{x^2-y^2}$ states near the Fermi level are the occupied spin-down $d_{x^2-y^2}$ states (denoted as $|d^{\downarrow}_{x^2-y^2,o}\rangle$) and the unoccupied spin-down d_{xy} states (denoted as $|d^{\downarrow}_{xy,u}\rangle$), which dominate the Fe-MAE, as circled in Fig. 4(e). The orientations of the spins in these states are the same. The Fe-MAE contributed by these two states is called spin-conserved MAE, denoted as $\mathrm{MAE}_{\mathrm{Fe,spin-conserved}}$. Here we have

$$\begin{aligned}&\mathrm{MAE}_{\mathrm{Fe,spin-conserved}}\\ &\quad= \xi^2 \sum_{o,u} \frac{|\langle d^{\downarrow}_{xy,u}|\hat{L}_z|d^{\downarrow}_{x^2-y^2,o}\rangle|^2 - |\langle d^{\downarrow}_{xy,u}|\hat{L}_x|d^{\downarrow}_{x^2-y^2,o}\rangle|^2}{E^{\downarrow}_{d_{xy,u}} - E^{\downarrow}_{d_{x^2-y^2,o}}},\end{aligned} \tag{10}$$

with the matrix elements [40]

$$\langle d_{xy}|\hat{L}_z|d_{x^2-y^2}\rangle = 2i \tag{11}$$

and

$$\langle d_{xy}|\hat{L}_x|d_{x^2-y^2}\rangle = 0, \tag{12}$$

the $\mathrm{MAE}_{\mathrm{Fe,spin-conserved}}$ can be simplified as

$$\mathrm{MAE}_{\mathrm{Fe,spin-conserved}} = \xi^2 \sum_{o,u} \frac{4}{E^{\downarrow}_{d_{xy,u}} - E^{\downarrow}_{d_{x^2-y^2,o}}}. \tag{13}$$

Clearly, the value of $\mathrm{MAE}_{\mathrm{Fe,spin-conserved}}$ is positive, which contributes to the positive Fe-MAE when U_{eff} is approximately 0.8 eV. However, when U_{eff} reaches 2 eV, the occupied spin-down $d_{x^2-y^2}$ states almost vanish on the valence band maximum (VBM), as seen in Fig. 4(f). This means that the SOC interaction between unoccupied spin-down d_{xy} states and occupied spin-down $d_{x^2-y^2}$ states almost disappears at this value of U_{eff}. Instead, the unoccupied spin-down d_{xy} states near the Fermi level mainly interact with the occupied spin-up $d_{x^2-y^2}$ states (denoted as $|d^{\uparrow}_{x^2-y^2,o}\rangle$) lying deeply in the valance bands, as circled in Fig. 4(f). This SOC interaction between these two states with antiparallel spins now dominates the Fe-MAE, and we denoted this MAE contribution as

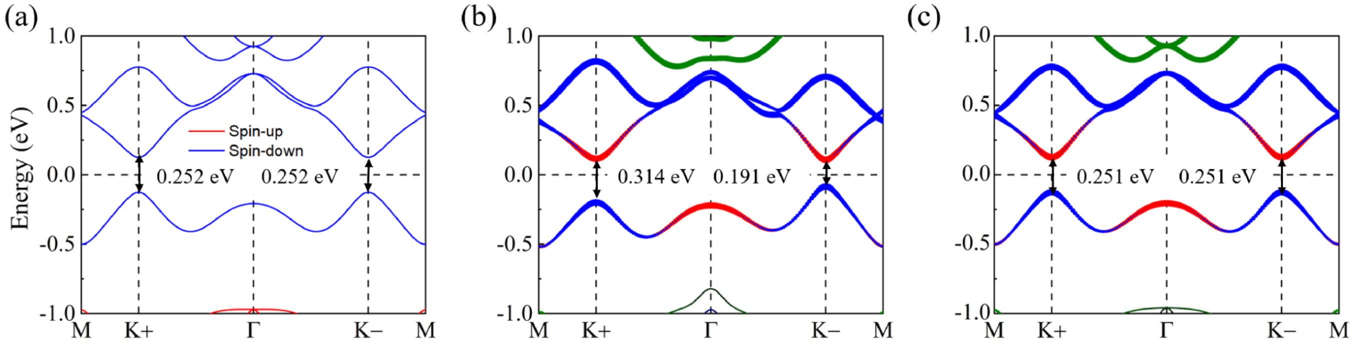

FIG. 5. The band structure of ferromagnetic SL H-FeBr$_2$ calculated with (a) spin-polarized case without including SOC, (b) out-of-plane magnetism with SOC, and (c) in-plane magnetization magnetism with SOC. In (b) and (c), the red, blue, and green dots represent Fe-A_1, Fe-E_1, and Fe-E_2 orbitals, respectively.

MAE$_{\mathrm{Fe,spin-flip}}$. It can be written as:

$$
\begin{aligned}
&\mathrm{MAE}_{\mathrm{Fe,spin-flip}}\\
&\quad= -\xi^2 \sum_{o,u} \frac{|\langle d^{\downarrow}_{xy,u}|\hat{L}_z|d^{\uparrow}_{x^2-y^2,o}\rangle|^2 - |\langle d^{\downarrow}_{xy,u}|\hat{L}_x|d^{\uparrow}_{x^2-y^2,o}\rangle|^2}{E^{\downarrow}_{d_{xy,u}} - E^{\uparrow}_{d_{x^2-y^2,o}}}\\
&\quad= -\xi^2 \sum_{o,u} \frac{4}{E^{\downarrow}_{d_{xy,u}} - E^{\uparrow}_{d_{x^2-y^2,o}}}. \qquad (14)
\end{aligned}
$$

The value of MAE$_{\mathrm{Fe,spin-flip}}$ is negative, which is now responsible for the negative Fe-MAE. Note that the d_{xy} and $d_{x^2-y^2}$ orbitals of Fe are degenerate in this case, we can perform the same analysis on the occupied spin-up d_{xy} states and unoccupied spin-down $d_{x^2-y^2}$ states of Fe near the Fermi level. After carefully examining the features of the DOS corresponding to these two orbitals, we found that the gap between the major peaks in the DOS becomes narrow with increasing U_{eff}. This directly contributes to the negative Fe-MAE value. In total, with increasing U_{eff}, the competition between MAE$_{\mathrm{Fe,spin-conserved}}$ and MAE$_{\mathrm{Fe,spin-flip}}$ causes the Fe-MAE to switch from positive values to negative values.

C. Evolution of band structures with electronic correlation strength

Let us again pay our attention to Figs. 4(e) and 4(f). It can be observed that the electronic structures associated with the Fe-d states vary greatly with U_{eff}, which could be reflected in the variation in the energy bands. Therefore, it is necessary to investigate the band structures with different U_{eff} values.

For comparison, the band structure of FM SL H-FeBr$_2$ at $U_{\mathrm{eff}} = 0.0$ eV was first examined. In this case, spin-polarized band structure without considering the SOC is plotted in Fig. 5(a). Clearly, the spin-up and spin-down channels are split, where the spin-down component dominates near the Fermi level. Meanwhile, the spin-down electronic band structure has a band gap of approximately 0.253 eV. Therefore, this system characterizes the FM half-semiconductor. In addition, the energy values of the VBM at $K+$ and $K-$ are equal. This scenario also occurs at the conduction band minimum (CBM) at the two k points. Thus, there are degenerate valleys in this energy band. This feature indicates that SL H-FeBr$_2$ is a 2D valleytronic material [41].

In fact, the SOC cannot be ignored in this system, so the SOC is taken into account in the following treatment. As mentioned before, the magnetization direction of this system can be in-plane or the out-of-plane. When the easy axis of magnetization is lying in-plane, the calculated energy bands show that the energy gaps at $K+$ and $K-$ are equal [Fig. 5(c)], and since the CBM (VBM) at $K+$ and $K-$ are degenerate, there is no spontaneous polarization of valleys. When we switch the easy axis to out-of-plane, the band-gap width at the $K+$ point is 0.314 eV and that at the $K-$ point is 0.191 eV [Figure 5(b)], showing the spontaneous polarization of the valleys. In this case the system is in the FV state. Strikingly, the difference in the band gap between $K+$ and $K-$ is 123 meV, which is larger than that of typical FV materials such as SL H-FeCl$_2$ (106 meV) [19], Nb$_3$I$_8$ (107 meV) [23], LaBr$_2$ (33 meV) [42], and MnPX$_3$ (43 meV) [43]. Apparently, the valley state strongly couples with the magnetization direction of SL H-FeBr$_2$, which is explained theoretically in Appendix A. According to previous reports [18,22], such FV materials with out-of-plane magnetization potentially possess topological nontrivial states. Therefore, in our following calculations, the magnetization orientation was set to be out-of-plane.

The evolution of electronic band structures with U_{eff} is investigated, and the representative band structures with different U_{eff} values are shown in Fig. 6. When U_{eff} increases to 0.5 eV, both the conduction bands and valence bands move toward the Fermi level, thereby reducing the band gaps at the $K+$ and $K-$ points. After increasing the value of U_{eff} to 0.6 eV, the band gap at the $K+$ point is still nonzero, but the band gap at the $K-$ point is closed [as shown in Fig. 6(c)]. Note that the system now has a Dirac-like band crossing at the $K-$ valley [44]. In this case, the system becomes the so-called half valley metal (HVM) [19], which can provide a massless elementary excitation that potentially contributes to well-behaved charge transport.

The band gap closed at the $K-$ point reopens when U_{eff} is slightly larger than 0.6 eV. Interestingly, at the $K-$ point, the low-lying E_1 orbital on the VBM shifts to the CBM, while the high-lying A_1 orbital on the CBM shifts down to the VBM [as shown in Fig. 6(d)]. Despite of this, the orbital composition of the energy band at the $K+$ point remains intact, forming a single-valley band-inverted state. When the value of U_{eff} is adjusted to approximately 0.9 eV, the band gap at the

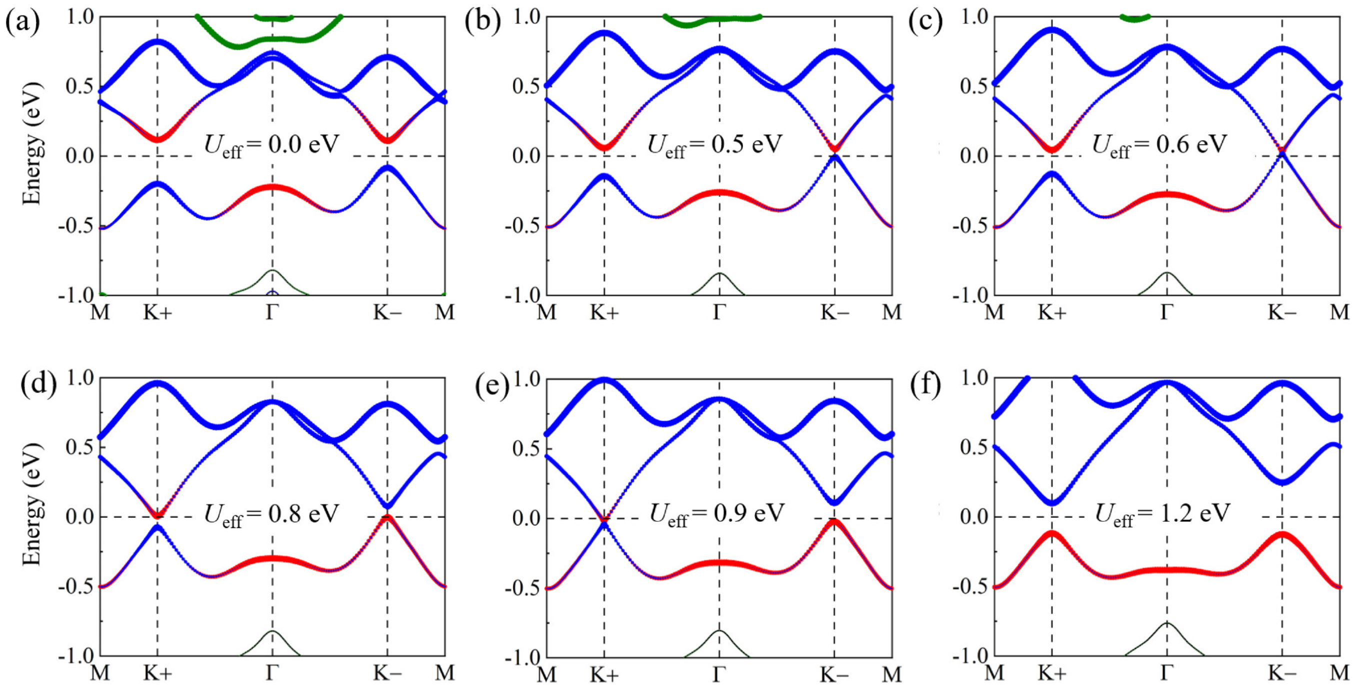

FIG. 6. The band structure of SL H-FeBr$_2$ calculated at (a) $U_{\text{eff}} = 0.0\,\text{eV}$, (b) $U_{\text{eff}} = 0.5\,\text{eV}$, (c) $U_{\text{eff}} = 0.6\,\text{eV}$, (d) $U_{\text{eff}} = 0.8\,\text{eV}$, (e) $U_{\text{eff}} = 0.9\,\text{eV}$, and (f) $U_{\text{eff}} = 1.2\,\text{eV}$. The red, blue, and green dots represent Fe-A_1, Fe-E_1, and Fe-E_2 orbitals, respectively.

$K-$ point reopens, and the band gap at the $K+$ point closes [as shown in Fig. 6(e)]. Compared to the case of $U_{\text{eff}} = 0.8\,\text{eV}$, the orbital composition of the CBM and VBM at the $K+$ point are reversed here. Meanwhile, we found that when U_{eff} is larger than 0.9 eV, the conduction band (valance band) near the Fermi level is contributed only by the orbitals of Fe-E_1 (A_1) [as shown in Fig. 6(f)]. If the value of U_{eff} is further increased, Fe-A_1 orbitals and Fe-E_1 orbitals are no longer entangled with each other on the conduction band (valance band) near the Fermi level. During this disentanglement process with increasing U_{eff}, the SOC interaction between the occupied spin-down $\text{Fe} - d_{xy}$ ($d_{x^2-y^2}$) orbitals on the valance bands near the Fermi level and the unoccupied spin-down $\text{Fe} - d_{x^2-y^2}$ (d_{xy}) orbitals on the conduction bands near the Fermi level weakens, which is the origin of the rapid switch in Fe-MAE.

To further characterize the effect of U_{eff} on valley-contrasting physics, the Berry curvature along the z direction was calculated based on the Kubo formula [45]:

$$\Omega_z(\boldsymbol{k}) = -\sum_n \sum_{n\neq n'} f_n \frac{2\text{Im}\langle\psi_{n\boldsymbol{k}}|v_x|\psi_{n'\boldsymbol{k}}\rangle\langle\psi_{n'\boldsymbol{k}}|v_y|\psi_{n\boldsymbol{k}}\rangle}{(E_n - E_{n'})^2}. \quad (15)$$

Here f_n is the Fermi-Dirac distribution function, E_n is the eigenvalue of Bloch state $|\psi_{n\boldsymbol{k}}\rangle$, and $v_{x/y}$ is the vector operator.

The k-resolved Berry curvatures for $U_{\text{eff}} = 0.0$ eV and $U_{\text{eff}} = 0.8$ eV are plotted in Figs. 7(a) and 7(b), respectively. In the case of $U_{\text{eff}} = 0.0$ eV, the Berry curvatures at $K+$ and $K-$ have peaks of opposite signs and different absolute values, which originates from the spontaneous breaking of time-reversal symmetry and spatial inversion symmetry. For such a system with a single valley band inversion, the Berry curvature peaks at $K+$ and $K-$ have the same sign when $U_{\text{eff}} = 0.8$ eV. In this case, the full-space integral over the Berry curvature yields a nonzero Chern number, which shows a topologically nontrivial character. To uncover the nature of this topologically nontrivial feature, we computed the edge states along the (100) direction in the system at $U_{\text{eff}} = 0.8$ eV. As shown in Fig. 7(c), there is a gapless chiral edge state, which simultaneously connects the valence band at $K+$ and the conduction band at $K-$. Such a gapless chiral edge state is the fingerprint of quantum anomalous Hall (QAH) states in topologically nontrivial systems with ferromagnetism [46,47]. Furthermore, the anomalous Hall conductivity (AHC) was calculated by the following formula [48,49]:

$$\sigma_{xy} = \frac{e^2}{h}\int_{\text{BZ}} \frac{d\boldsymbol{k}}{(2\pi)^2}\Omega_z(\boldsymbol{k}). \quad (16)$$

As shown in Fig. S2 in the Supplemental Material [39]), the AHC in the energy gap is $-\frac{e^2}{h}$, confirming a QAH state with a Chern number of $C = -1$ in this system. Note that this single-valley band-inverted state with the QAH effect is the so-called QAVH state [19]. Therefore, when the electron correlation strength is adequate, SL H-FeBr$_2$ can possess a QAVH state, which has potential applications for the spintronic devices.

In principle, the presence of the QAVH state in the system is relevant to the value of U_{eff}. We thus carefully search for the range of U_{eff} in which the QAVH effect appears in the system. Figure 7(d) displays the topological phase diagram, from which it can be seen that the QAVH state exists in the range of U_{eff} varying from 0.6 to 0.9 eV. As we know, the QAVH state can only survive when the system hosts PMA. The value of U_{eff} corresponding to the QAVH state ranges

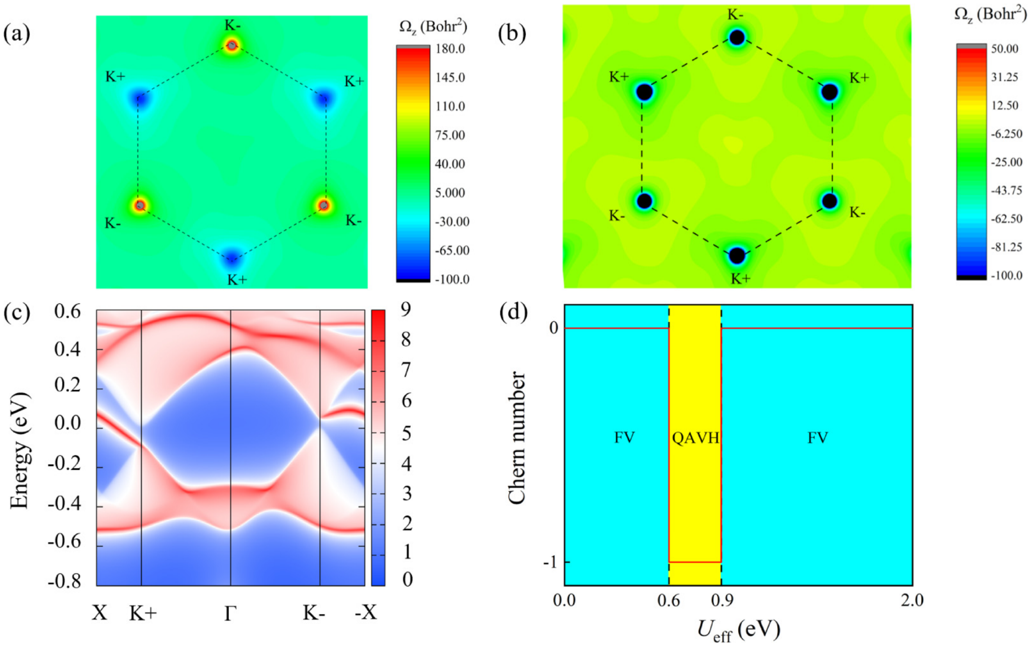

FIG. 7. The Berry curvature of SL H-FeBr$_2$ in the 2D Brillouin zone calculated at (a) $U_{\mathrm{eff}} = 0.0$ eV and (b) $U_{\mathrm{eff}} = 0.8$ eV; both units of Berry curvature in (a) and (b) are Bohr^2. (c) Topological edge state of SL H-FeBr$_2$ along the (100) direction calculated at $U_{\mathrm{eff}} = 0.8$ eV; (d) topological phase diagram of SL H-FeBr$_2$ with varied U_{eff}.

from 0.6 to 0.9 eV, which belongs to the U_{eff} value interval of PMA (from 0.1 to 1.0 eV). Thus, the QAVH state could naturally exist in this system without external magnetic fields.

D. Discussion

We are now curious to see whether the behavior of U_{eff}-dependent MAE in SL H-FeBr$_2$ is present in SL H-FeX$_2$ (X = Cl, I), which are the counterparts of SL H-FeBr$_2$. To this end, the total MAEs of SL H-FeX$_2$ (X = Cl, I) in the FM state were computed, which are all plotted in Figs. 8(a)–8(c). Obviously, as the value of U_{eff} increases in the considered range, all of the total MAEs of SL H-FeX$_2$ (X = Cl, I) experience sensitive changes.

Commonly, the total MAE of SL H-FeX$_2$ (X = Cl, I) shows a rapid decrease after U_{eff} reaches a critical magnitude. To understand this common feature, the element-resolved MAEs of SL H-FeX$_2$ (X = Cl, Br, I) under different values of U_{eff} are plotted in Figs. 8(d)–8(f). It can be observed that when U_{eff} is small, the Fe-MAEs of SL H-FeX$_2$ (X = Cl, Br, I) remain almost constant. However, after U_{eff} reaches a critical value, the Fe-MAEs suddenly decrease with U_{eff}. Similarly to the case in SL H-FeBr$_2$, these common features in the Fe-MAE of SL H-FeX$_2$ (X = Cl, Br, I) all originate from the disentanglement between the Fe-A_1 and Fe-E_1 orbitals, which are all reflected in the evolution of their band structures with U_{eff} (as shown in Fig. S3 and S5 in the Supplemental Material [39]). This disentanglement weakens the SOC interaction between occupied Fe- d_{xy} ($d_{x^2-y^2}$) orbitals at the VBM and unoccupied Fe-$d_{x^2-y^2}$ (d_{xy}) orbitals at the CBM, giving rise to a strong decrease in the Fe-MAE. Notably, if the magnetization directions of all SL H-FeX$_2$ (X = Cl, Br, I) compounds are forced to be out-of-plane, then the topological phase transitions might commonly occur during the continuous tuning of U_{eff}, giving rise to HVM and QAVH states.

In addition to the common features mentioned above, the MAEs of different members in SL H-FeX$_2$ (X = Cl, Br, I) also show significant differences. First, the MAEs of SL H-FeCl$_2$ and H-FeBr$_2$ exhibit transitions between positive and negative MAEs with increasing U_{eff}, which corresponds to the reversal of their magnetization behaviors between out-of-plane and in-plane, but the MAE of SL H-FeI$_2$ does not behave in this way. Second, when the value of U_{eff} is small, the MAEs from X (X = Br,I) elements (denoted as X-MAE) in both SL H-FeBr$_2$ and H-FeI$_2$ increase significantly with increasing U_{eff}; as the U_{eff} value continues to rise, the X-MAEs (X = Br, I) of both systems increase slowly. However, the Cl-MAE of SL H-FeCl$_2$ is not sensitive to U_{eff} in the above-mentioned process of increasing U_{eff}, as shown in Figs. 8(d)–8(f). Apparently, the halogen atoms of Br and I tend to provide negative MAEs. Among them, the amplitude of the negative I-MAE in H-FeI$_2$ is larger than that of the positive Fe-MAE, so the total MAE of H-FeI$_2$ is always negative. However, in SL H-FeCl$_2$, the total MAE of H-FeCl$_2$ is almost entirely contributed by Fe-MAE since Cl atoms hardly contribute to MAE. Therefore, the evolution behavior of total MAE in SL H-FeCl$_2$ is dominated by Fe-MAE. Based on these calculations, we found that the heavier halogen atoms would give more negative contribution to the total MAE.

Finally, similarly to the case of SL H-FeBr$_2$, in SL H-FeX$_2$ (X = Cl, I) with out-of-plane magnetization, we also observed chiral edge states connecting the conduction bands and valance bands, as well as an AHC of $-\frac{e^2}{h}$ lying in the energy gap (see Fig. S4 and S6 in the Supplemental Material [39]) in specific intervals of U_{eff}. These characteristics

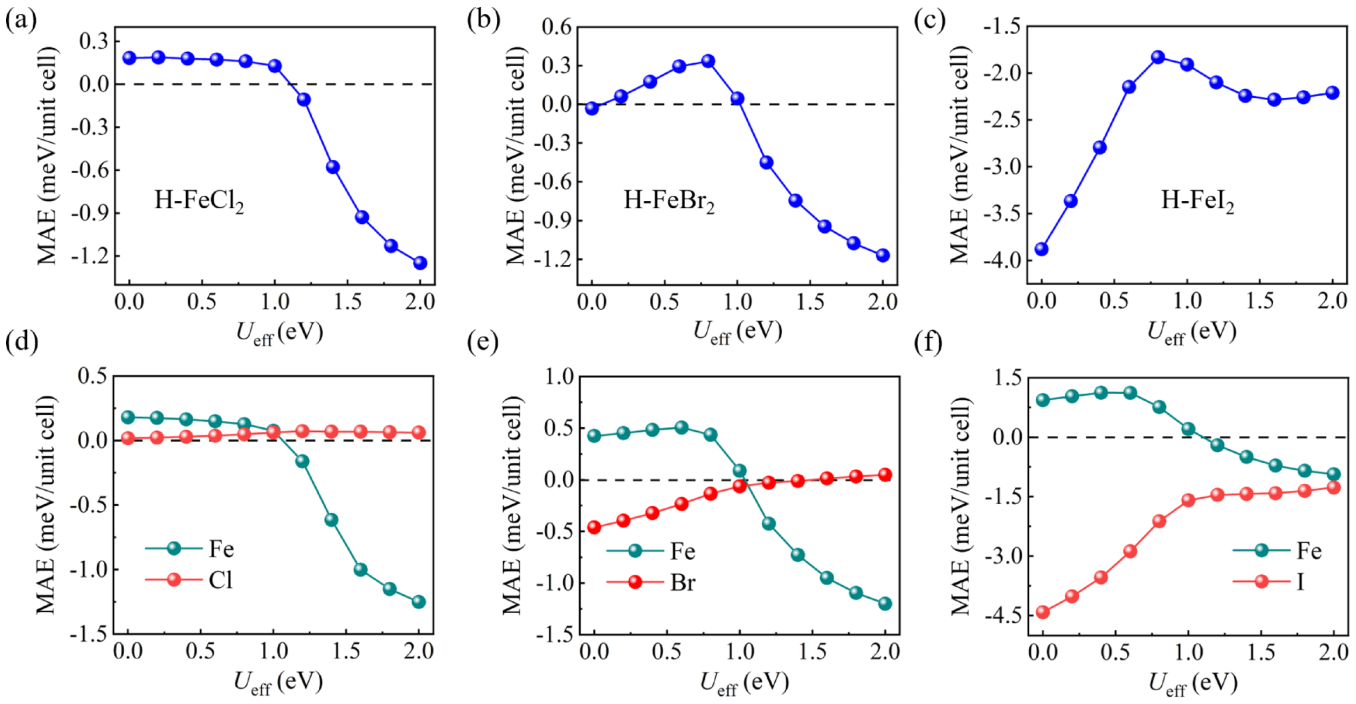

FIG. 8. Evolution of total MAE of (a) SL H-FeCl$_2$, (b) SL H-FeBr$_2$, and (c) SL H-FeI$_2$. The evolution of element-resolved MAE of (d) SL H-FeCl$_2$, (e) SL H-FeBr$_2$, and (f) SL H-FeI$_2$ are also given.

confirm the QAH states with Chern numbers being C = -1. We emphasize that these common features of correlation-driven electronic topology stem from the Fe-d orbitals, which dominate the low-energy states of SL H-FeX$_2$ (X = Cl, Br, I).

IV. CONCLUSION

We investigated the evolution of MAE as well as electronic structures of SL H-FeBr$_2$ under varying correlation strengths, quantified as $U_{\rm eff}$ imposed on Fe ions. It is found that the MAE decreases after its increase with $U_{\rm eff}$, and the transition between negative and positive MAEs reflects the switching between out-of-plane magnetization and in-plane magnetization. This nonmonotonic evolution behavior of MAE stems from the competition of element-resolved MAE between Fe and Br. The evolution of element-resolved MAE was found to arise from the variation of SOC interaction between different orbitals. Further investigation revealed that as $U_{\rm eff}$ increases, the energy bands of SL H-FeBr$_2$ at $K+$ and $K-$ invert in turn, giving rise to topological phase transitions, and a QAVH state with chiral edge states was predicted. By comparing the MAE evolution behaviors of different members in the SL H-FeX$_2$ (X = Cl, Br, I) family, the underlying mechanisms of the universality and specificity of MAE evolution behavior are provided. Our study has deepened the understanding of correlation-induced electronic structural transition of the SL H-FeX$_2$ (X = Cl, Br, I) family, which would open new perspectives of possible spintronics and valleytronics applications on nanoelectronic devices based on these materials.

ACKNOWLEDGMENTS

The author sincerely thanks Professor Wenhui Duan, Professor Yong Xu, Haowei Chen, Zhiming Xu, and Feng Xue for helpful discussions.

APPENDIX A: THE MAGNETO-VALLEY COUPLING IN SL *H*-FeBr$_2$

Basically, the coupling of spontaneous valley polarization and magnetization direction stems from the existence of SOC. To illustrate this, we express the SOC Hamiltonian as:

$$\hat{H}_{\rm SOC} = \lambda \hat{L} \cdot \hat{S}. \tag{A1}$$

Here λ represents the strength of SOC, while $\hat{L}$ and $\hat{S}$ are the orbital angular moment and spin angular moment respectively. The SOC can be decoupled as

$$\hat{H}_{\rm SOC} = \hat{H}^0_{\rm SOC} + \hat{H}^1_{\rm SOC}, \tag{A2}$$

where $\hat{H}^0_{\rm SOC}$ represents the interaction between the same spin states, and $\hat{H}^1_{\rm SOC}$ describes the interaction between the states with opposite spin angular moments. Here $\hat{H}^0_{\rm SOC}$ and $\hat{H}^1_{\rm SOC}$ are expressed as [40,50]:

$$\hat{H}^0_{\rm SOC} = \lambda \hat{S}_{z'} \times \left(\hat{L}_z\cos\theta + \frac{1}{2}\hat{L}_+e^{-i\phi}\sin\theta + \frac{1}{2}\hat{L}_-e^{i\phi}\sin\theta\right), \tag{A3}$$

$$\hat{H}^1_{\mathrm{SOC}} = \frac{\lambda}{2}(\hat{S}_{+'} + \hat{S}_{-'}) \times \left(-\hat{L}_z \sin\theta + \frac{1}{2}\hat{L}_+ e^{-i\phi}\cos\theta + \frac{1}{2}\hat{L}_- e^{i\phi}\cos\theta \right). \tag{A4}$$

In the above expressions, two Cartesian coordinate systems (x, y, z) and (x', y', z') are defined for the orientation of $\hat{L}$ and $\hat{S}$, respectively. These two Cartesian coordinate systems are linked by two polar angles, θ and ϕ. And

$$\hat{L}_\pm = \hat{L}_x \pm i\hat{L}_y, \tag{A5}$$

$$\hat{S}_{\pm'} = \hat{S}_{x'} \pm i\hat{S}_{y'}. \tag{A6}$$

Because both CBM and VBM belong to the same spin channel, only $\hat{H}^0_{\mathrm{SOC}}$ takes effect and $\hat{H}^1_{\mathrm{SOC}}$ can be neglected in the following analysis.

The orbital components of each valley are plotted in Fig. 5(b). At $K+$ and $K-$, the CBMs are mainly contributed by Fe-A_1 orbitals, while the VBMs are jointly dominated by Fe-E_1 orbitals. Moreover, as shown in Fig. 5(a), both the CBM and VBM belong to the spin-down channel. Therefore, based on the local C_{3h} k-vector group at $K+$ and $K-$, the basis functions of CBM and VBM are chosen as:

$$\left|\Psi_c^\tau\right\rangle = |d_{z^2}\rangle \otimes |\downarrow\rangle, \tag{A7}$$

$$\left|\Psi_v^\tau\right\rangle = \frac{1}{\sqrt{2}}(|d_{x^2-y^2}\rangle + i\tau d_{xy}\rangle) \otimes |\downarrow\rangle, \tag{A8}$$

where $\tau = \pm 1$ refers to the valley index corresponding to $K+/K-$. For out-of-plane magnetization, $\theta = 0$, we have

$$\hat{H}_{\mathrm{out-of-plane}} \approx \hat{H}_{\mathrm{SOC}}(\theta = 0) = \lambda \hat{L}_z \hat{S}_{z'}. \tag{A9}$$

As a result, the energy shifting of CBM and VBM caused by SOC are respectively

$$E_c^\tau = \left\langle \psi_c^\tau \middle| \hat{H}_{\mathrm{SOC}}(\theta = 0) \middle| \psi_c^\tau \right\rangle \tag{A10}$$

and

$$E_v^\tau = \left\langle \psi_v^\tau \middle| \hat{H}_{\mathrm{SOC}}(\theta = 0) \middle| \psi_v^\tau \right\rangle, \tag{A11}$$

The energy difference at either the CBM or the VBM between $K+$ and $K-$ can be derived as:

$$\Delta E_c = E_c^{K+} - E_c^{K-} = 0, \tag{A12}$$

$$\begin{aligned} \Delta E_v &= E_v^{K+} - E_v^{K-} \\ &= i\langle d_{x^2-y^2}|\hat{H}_{\mathrm{SOC}}|d_{xy}\rangle - i\langle d_{xy}|\hat{H}_{\mathrm{SOC}}|d_{x^2-y^2}\rangle \\ &= 4\lambda, \end{aligned} \tag{A13}$$

where we have used [40]

$$\hat{L}_z|d_{x^2-y^2}\rangle = 2i|d_{xy}\rangle \tag{A14}$$

and

$$\hat{L}_z|d_{xy}\rangle = -2i|d_{x^2-y^2}\rangle. \tag{A15}$$

Thus, the existence of valley polarization has been demonstrated by the existence of nonzero ΔE_v. It can be clearly seen that the energy difference at each valley is solely contributed by valance bands, instead of conduction bands, which is consistent with our calculation results.

For the case of in-plane magnetization, $\theta = \frac{\pi}{2}$, we have

$$\hat{H}_{\mathrm{in-plane}} \approx \frac{\lambda}{2}(\hat{L}_+ e^{-i\phi} + \hat{L}_- e^{+i\phi}) \cdot \hat{S}_{z'}. \tag{A16}$$

In this case, it can be derived that both ΔE_c and ΔE_v are zero, revealing the absence of valley polarization. As a result, being mediated by SOC, the valley polarization is coupled with magnetization direction.

[1] Z. He and G. Xu, Phys. Rev. B **104**, 235108 (2021).

[2] Y. Wang, Z. Wang, Z. Fang, and X. Dai, Phys. Rev. B **91**, 125139 (2015).

[3] S. Sorella, K. Seki, O. O. Brovko, T. Shirakawa, S. Miyakoshi, S. Yunoki, and E. Tosatti, Phys. Rev. Lett. **121**, 066402 (2018).

[4] W. Chen and J. L. Lado, Phys. Rev. Lett. **122**, 016803 (2019).

[5] M. Rösner and J. L. Lado, Phys. Rev. Res. **3**, 013265 (2021).

[6] S. Keshavarz, J. Schött, A. J. Millis, and Y. O. Kvashnin, Phys. Rev. B **97**, 184404 (2018).

[7] K. Misumi, T. Kaneko, and Y. Ohta, Phys. Rev. B **95**, 075124 (2017).

[8] L. Ke and M. I. Katsnelson, npj Comput. Mater. **7**, 4 (2021).

[9] A. X. Gray, J. Jeong, N. P. Aetukuri, P. Granitzka, Z. Chen, R. Kukreja, D. Higley, T. Chase, A. H. Reid, H. Ohldag, M. A. Marcus, A. Scholl, A. T. Young, A. Doran, C. A. Jenkins, P. Shafer, E. Arenholz, M. G. Samant, S. S. P. Parkin, and H. A. Dürr, Phys. Rev. Lett. **116**, 116403 (2016).

[10] C. De Franco, L. F. Tocchio, and F. Becca, Phys. Rev. B **98**, 075117 (2018).

[11] Q. Yao, J. Li, and Q. Liu, Phys. Rev. B **104**, 035108 (2021).

[12] A. Raja, A. Chaves, J. Yu, G. Arefe, H. M. Hill, A. Rigosi, T. C. Berkelbach, P. Nagler, C. Schüller, and T. Korn, Nat. Commun. **8**, 15251 (2017).

[13] M. Utama, H. Kleemann, W. Zhao, C. S. Ong, F. H. da Jornada, D. Y. Qiu, H. Cai, H. Li, R. Kou, S. Zhao *et al.*, Nat. Electron. **2**, 60 (2019).

[14] L. Waldecker, A. Raja, M. Rösner, C. Steinke, A. Bostwick, R. J. Koch, C. Jozwiak, T. Taniguchi, K. Watanabe, E. Rotenberg, T. O. Wehling, and T. F. Heinz, Phys. Rev. Lett. **123**, 206403 (2019).

[15] L. Meng, Z. Zhou, M. Xu, S. Yang, and Y. Gong, Nat. Commun. **12**, 809 (2021).

[16] A. Karbalaee Aghaee, S. Belbasi, and H. Hadipour, Phys. Rev. B **105**, 115115 (2022).

[17] S. Li, Q. Wang, C. Zhang, P. Guo, and S. A. Yang, Phys. Rev. B **104**, 085149 (2021).

[18] X. Kong, L. Li, L. Liang, F. M. Peeters, and X. J. Liu, Appl. Phys. Lett. **116**, 192404 (2020).

[19] H. Hu, W.-Y. Tong, Y.-H. Shen, X. Wan, and C.-G. Duan, npj Comput. Mater. **6**, 129 (2020).

[20] P. Zhao, Y. Dai, H. Wang, B. Huang, and Y. Ma, Chem. Phys. Mater. **1**, 56 (2022).

[21] W. Y. Tong, S. J. Gong, X. Wan, and C. G. Duan, Nat. Commun. **7**, 13612 (2016).

[22] S.-D. Guo, J.-X. Zhu, M.-Y. Yin, and B.-G. Liu, Phys. Rev. B **105**, 104416 (2022).

[23] R. Peng, Y. Ma, X. Xu, Z. He, B. Huang, and Y. Dai, Phys. Rev. B **102**, 035412 (2020).

[24] G. Kresse and J. Furthmüller, Phys. Rev. B **54**, 11169 (1996).

[25] J. P. Perdew, K. Burke, and M. Ernzerhof, Phys. Rev. Lett. **77**, 3865 (1996).

[26] S. L. Dudarev, G. A. Botton, S. Y. Savrasov, C. J. Humphreys, and A. P. Sutton, Phys. Rev. B **57**, 1505 (1998).

[27] S. Grimme, J. Antony, S. Ehrlich, and H. Krieg, J. Chem. Phys. **132**, 154104 (2010).

[28] A. A. Mostofi, J. R. Yates, G. Pizzi, Y.-S. Lee, I. Souza, D. Vanderbilt, and N. Marzari, Comput. Phys. Commun. **185**, 2309 (2014).

[29] Q. S. Wu, S. N. Zhang, H. F. Song, M. Troyer, and A. A. Soluyanov, Comput. Phys. Commun. **224**, 405 (2018).

[30] Qurat-ul-ain, D. Odkhuu, S. H. Rhim, and S. C. Hong, Phys. Rev. B **101**, 214436 (2020).

[31] V. Antropov, L. Ke, and D. Åberg, Solid State Commun. **194**, 35 (2014).

[32] J. Zhang, P. V. Lukashev, S. S. Jaswal, and E. Y. Tsymbal, Phys. Rev. B **96**, 014435 (2017).

[33] R. Skomski, A. Kashyap, and A. Enders, J. Appl. Phys. **109**, 07E143 (2011).

[34] J. B. Goodenough, Phys. Rev. **100**, 564 (1955).

[35] J. Kanamori, J. Phys. Chem. Solids **10**, 87 (1959).

[36] Z. Xu, M. Ye, J. Li, W. Duan, and Y. Xu, Phys. Rev. B **105**, 085129 (2022).

[37] D.-s. Wang, R. Wu, and A. J. Freeman, Phys. Rev. B **47**, 14932 (1993).

[38] H. Chen, P. Tang, and J. Li, Phys. Rev. B **103**, 195402 (2021).

[39] See Supplemental Material at http://link.aps.org/supplemental/10.1103/PhysRevB.106.125122 for more details about the orbital-resolved MAE, energy band structures, Berry curvature distributions, anomalous hall conductivity, and topological edge states of single-layer H-$\mathrm{FeX_2}$($X = \mathrm{Cl}$, Br, I),

[40] M.-H. Whangbo, H. Xiang, H.-J. Koo, E. E. Gordon, and J. L. Whitten, Inorg. Chem. **58**, 11854 (2019).

[41] J. R. Schaibley, H. Yu, G. Clark, P. Rivera, J. S. Ross, K. L. Seyler, W. Yao, and X. Xu, Nat. Rev. Mater. **1**, 16055 (2016).

[42] P. Zhao, Y. Ma, C. Lei, H. Wang, and Y. Dai, Appl. Phys. Lett. **115**, 261605 (2019).

[43] X. Li, T. Cao, Q. Niu, J. Shi, and J. Feng, Proc. Natl. Acad. Sci. USA **110**, 3738 (2013).

[44] N. P. Armitage, E. J. Mele, and A. Vishwanath, Rev. Mod. Phys. **90**, 015001 (2018).

[45] D. J. Thouless, M. Kohmoto, M. P. Nightingale, and M. den Nijs, Phys. Rev. Lett. **49**, 405 (1982).

[46] C.-X. Liu, S.-C. Zhang, and X.-L. Qi, Annu. Rev. Condens. Matter Phys. **7**, 301 (2016).

[47] K. He, Y. Wang, and Q.-K. Xue, Annu. Rev. Condens. Matter Phys. **9**, 329 (2018).

[48] T. Jungwirth, Q. Niu, and A. H. MacDonald, Phys. Rev. Lett. **88**, 207208 (2002).

[49] Y. Yao, L. Kleinman, A. H. MacDonald, J. Sinova, T. Jungwirth, D.-s. Wang, E. Wang, and Q. Niu, Phys. Rev. Lett. **92**, 037204 (2004).

[50] M.-H. Whangbo, E. E. Gordon, H. Xiang, H.-J. Koo, and C. Lee, Acc. Chem. Res. **48**, 3080 (2015).